ELEKTROTEHNIŠKI VESTNIK 82(4): 183-190, 2015
ORIGINAL SCIENTIFIC PAPER

A complex Hydro-Power Plant Dynamic Model Integrated into the Electrical Network

Klemen Nagode[1], Boštjan Murovec[2]

[1] *Savske elektrarne Ljubljana d.o.o., Gorenjska cesta 46, 1215 Medvode, Slovenija*
[2] *Univerza v Ljubljani, Fakulteta za elektrotehniko, Tržaška 25, 1000 Ljubljana, Slovenija*
E-mail: klemen.nagode@sel.si

Abstract. The paper presents a complex modelling of a hydro-power plant synchronized with an electrical network. A dynamic performance model of a synchronous generator, Kaplan turbine, turbine controller, excitation system, automatic voltage regulator, transformer and simplified electrical network is designed in accordance with the IEEE recommended practices and standards. The developed model which is validated with the *in situ* measurements taken on the Mavčiče hydro-power plant and nearby 110 kV Slovenian electrical network shows a great matching of the characteristics. An important property of the model is its ability to simulate the various types of the power-system operation and the impact of the hydro-power plant control systems on the electrical network, especially the hazard scenarios that cannot be tested on a real power system.

Keywords: hydro-power plant, simulation, excitation system, turbine controller, power system

Kompleksen dinamičen model hidroelektrarne, vključene v električno omrežje

V članku je predstavljen kompleksen model hidroelektrarne, sinhronizirane z električnim omrežjem. Model obravnava dinamične lastnosti sinhronskega generatorja, Kaplanove turbine, turbinskega regulatorja, vzbujalnega sistema, avtomatskega regulatorja napetosti, energetskega transformatorja in poenostavljenega električnega omrežja skladno s standardi IEEE in prakso. Zasnovani dinamični model je validiran z meritvami na hidroelektrarni Mavčiče in bližnjim 110 kV električnim omrežjem ter izkazuje dobro ujemanje dinamičnih lastnosti z realnim sistemom. Prednostna lastnost predstavljenega modela je v možnosti simulacije različnih obratovalnih stanj, prehodnih pojavov, vpliva regulacijskih sistemov na električno omrežje ter proučevanje hazardnih scenarijev, katerih na realnem energetskem sistemu ni mogoče izvesti zaradi obratovalnih omejitev.

1 INTRODUCTION

Nowadays, the hydro-power plants (HPP) present an important worldwide source of the renewable energy. In order to foster further the power-system development, an appropriate modelling of the essential HPP components is necessary in order to gain an advanced knowledge of their dynamic performance. This paper focuses on a model, developed to cover the following elements of an underlying power system:

1. A synchronous generator with a salient-pole rotor.
2. A static excitation system based on the IEEE ST6B type [1] that includes an automatic voltage regulator (AVR) with a reactive-power controller in accordance with the IEEE standard [1].
3. A turbine controller with the main active-power Proportional-Integral-Derivative (PID) control loop, guide-vane opening and runner-blade opening sub-control loops.
4. Characteristics of the Kaplan water-turbine dynamics with servomotors.
5. A 119/10.5 kV block transformer.
6. 110 kV power lines presented with three-phase PI-modelled sections.
7. Three-phase voltage sources (determined with the short-circuit power) connected to the power lines.
8. Three-phase parallel RLC loads connected to the power lines.

In our case, the platform for the simulation is Matlab with Simulink in conjunction with the SimPowerSystems analysis tool.

In the literature, different approaches are used to study the power-system dynamic models. In [2]-[4], the authors conduct a comprehensive survey of the load-frequency control strategies and HPP models. The latter are classified as linear (non-elastic) models and nonlinear with an elastic water-column effect. The classical control methodologies include the PID controllers with the Bode diagram, Nyquist diagram and root-locus analysis. These approaches are of a great practical value for the implementation, however, they

Received 15 May 2015
Accepted 30 June 2015

show a poor dynamic performance in the case of the parameter deviations or nonlinearities. The modern control techniques use more complex algorithms like the adaptive and variable-structure methods as well as intelligent and robust approaches. These are more adequate in the case of uncertainties, disturbances, load variations and errors in modelling.

In [5]-[6] the authors propose a load-frequency control of a multi-area source with an optimal output feedback controller and neuro-fuzzy hybrid intelligent PI control. The drawback of their contribution is that the models of the hydro, steam and gas turbines used in the simulation are too much simplified.

A fractional-order PID controller for the AVR system using a chaotic multi-objective optimization is studied in [7]. The authors rely only on the first-order transfer functions for the exciter and generator and neglect the turbine and electrical network integration.

A simulation model of the Shkopeti HPP, Albania, is introduced by Prillwitz et al. [8]. A comparison between the HPP model and the measured signals is presented, however, the impact on the electrical network is not included.

The International Electrotechnical Commission (IEC) and the Institute of Electrical and Electronics Engineers (IEEE) standards [1], [9]-[13] describe the recommended approaches to design and develop various turbine, excitation-system, generator and load models. These standards also define the guidelines for the functional verification and fulfilment of the tender guarantees. Notwithstanding their important role, it is often very difficult to extract adequate recommendations in the development.

The impact of a specific load (charging of electrical vehicles) on the power network stability is addressed in [14] where the authors predict the daily voltage fluctuations in 2030 for the case that 10 % of the vehicles would rely on the electrical power. In [15]-[16], the authors optimize the reactive-power compensation and active-power scheduling but with no consideration of the features of the power-generation process.

In this paper, a complete dynamic model of the Mavčiče HPP (on the Sava river, Slovenia) together with its subsystems is proposed in Sec. 2. Compared with the previously described researches, this model integrates the functional components of the entire HPP production and transmission system based on the real power-system measurements. Moreover, the synchronous generator, excitation system and water turbine with a controller connected to the 110 kV network include the non-linear dynamics that reflect the characteristics of a real power system. In Sec. 3, the simulation results and validation of the model based on real measurements are described. The impact of the HPP operation on the 110 kV electrical network is presented in Sec. 4. Conclusions are summarized in Sec. 5.

2 HPP MODELLING

A typical interconnection diagram of HPP with a synchronous machine is depicted in Fig. 1. The vital subsystems included in the simulation are presented with solid lines, whereas the neglected functional parts are marked with dashed lines.

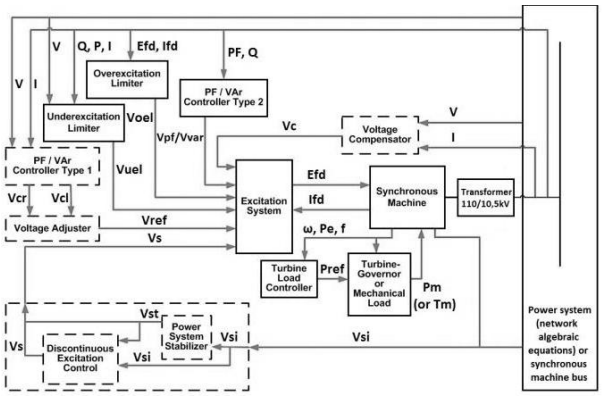

Figure 1. Typical interconnection system of a synchronous machine [13].

2.1 Synchronous generator

A three-phase salient-pole synchronous generator with the nominal power of 25 MVA, voltage of 10.5 kV and power factor of $cos\varphi$=0.8 is included in the model. A dynamic model with the stator variables within the reference frame fixed in the rotor (SimPowerSystem synchronous machine per unit (p.u.) standard block) is presented with the Park's voltage differential equations [17] in the following expanded form (1-7):

$$u_{qs}^{r} = -R_s \cdot i_{qs}^{r} + \omega_r \cdot \lambda_{ds}^{r} + \frac{d\lambda_{qs}^{r}}{dt} \quad (1)$$

$$u_{ds}^{r} = -R_s \cdot i_{ds}^{r} - \omega_r \cdot \lambda_{qs}^{r} + \frac{d\lambda_{ds}^{r}}{dt} \quad (2)$$

$$u_{0s} = -R_s \cdot i_{0s} + \frac{d\lambda_{0s}}{dt} \quad (3)$$

$$u_{fd}^{'r} = R_{fd}^{'} \cdot i_{fd}^{'r} + \frac{d\lambda_{fd}^{'r}}{dt} \quad (4)$$

$$u_{kd}^{'r} = R_{kd}^{'} \cdot i_{kd}^{'r} + \frac{d\lambda_{kd}^{'r}}{dt} \quad (5)$$

$$u_{kq1}^{'r} = R_{kq1}^{'} \cdot i_{kq1}^{'r} + \frac{d\lambda_{kq1}^{'r}}{dt} \quad (6)$$

$$u_{kq2}^{'r} = R_{kq2}^{'} \cdot i_{kq2}^{'r} + \frac{d\lambda_{kq2}^{'r}}{dt} \quad (7)$$

where u^{r}_{qs} and u^{r}_{ds} denote the stator voltages in the q and d direction. Voltage u_{0s} is related to the three-phase stationary voltages independent of reference-frame speed ω that is equal to rotor speed ω_r at transformation to the rotor reference frame. Equ. (4-7) describes the rotor excitation-field voltage $u^{'r}_{fd}$ and damper winding voltages: $u^{'r}_{kd}$ in the d axis and $u^{'r}_{kq1}$ and $u^{'r}_{kq2}$ in the q axis. The indices referring to voltage u, resistance R, current i, and magnetic flux linkage λ, indicate the q - q

axis, d - d axis, s - stator of the generator, f - rotor-field winding and k - rotor-damper winding.

The model of the synchronous generator includes the manufacturer's [18] real values for the synchronous, transient and subtransient reactances as well as short-circuit time constants (T_d', T_d'' and T_q'') for the d and q directions.

The stator resistance per unit is calculated as:

$$R_{spu} = \frac{R_s}{Z_b} \tag{8}$$

with phase stator resistance R_s and base impedance Z_b expressed in (9):

$$Z_b = \frac{U_b^2}{S_b} \tag{9}$$

where U_b denotes the base phase voltage and phase apparent power S_b.

Inertia constant H [19] included in the turbine-generator rotor model is expressed in (10):

$$H = 5{,}48 \cdot 10^{-9} \frac{J \cdot n^2}{S_n} \tag{10}$$

where J is the inertia of the rotor, n is the synchronous speed (in revolutions per minute) and S_n is the generator nominal apparent power.

2.2 Static excitation system

A dynamic model of the static excitation system with an overexcitation limiter "OverexcLim2", underexcitation limiter "UnderexcLimIEEE2" and reactive-power controller VAR Type II is realized (Fig. 2) based on the IEEE ST6B Type [1]. The error signal of the voltage regulator (input in the PI controller) is calculated with (11):

$$e = \max(V_{uel}; V_{var} + V_{ref} - V_c - V_{oel}) + V_s \tag{11}$$

where V_{uel}, V_{var}, V_{oel} and V_s denote the output of the underexcitation limiter, reactive-power controller, overexcitation limiter and power-system stabilizer, respectively.

Parameter V_{ref} denotes the voltage-reference setpoint and V_c denotes the low-pass filtered feedback voltage from the generator terminals.

The output of the PI controller enters the inner loop which includes a field-voltage regulator with a proportional control (gain K_m) and pre-control loop (gain K_{ff}). The output of the controller is further calculated:

$$u = \min\Big(\big(I_{lr} \cdot K_{ci} - I_{fd}\big) \cdot K_{lr}; \big(u_{PI} - E_{fd} \cdot \frac{K_g}{T_g \cdot s + 1}\big) \cdot K_m + u_{PI} \cdot K_{ff}\Big) \cdot V_b \tag{12}$$

The first argument of the min function in Equ. (12) denotes the field-current limiter with limitation parameter I_{lr} and gains K_{ci} and K_{lr}. A low-pass filter for the field voltage with time constant T_g and gain K_g is used for the error-signal calculation.

2.3 Water turbine with a digital turbine controller

A dynamic model of a double-regulated (Kaplan) water turbine with a turbine controller is implemented. The controller inputs are: the reference of active power P_{ref}, active power P_e, speed of the generator w, speed reference w_{ref}, net head dH, opening position of guide vane Y_v and opening position of the runner Y_g. The output of the PID controller indicates setpoint opening for guide vane and runner that change water flow through the turbine. The main PID controller error signal is expressed as (13):

$$e_{PID} = w_{ref} - w - R \cdot (P_{ref} - P_e) \tag{13}$$

where R denotes the steady state droop parameter.

Referring to the optimal operating efficiency without cavitation, appropriate Y_g/Y_v ratio is considered that is a nonlinear function of the head:

$$Y_g = f(dH, Y_v) \tag{14}$$

realized with a 2D lookup table.

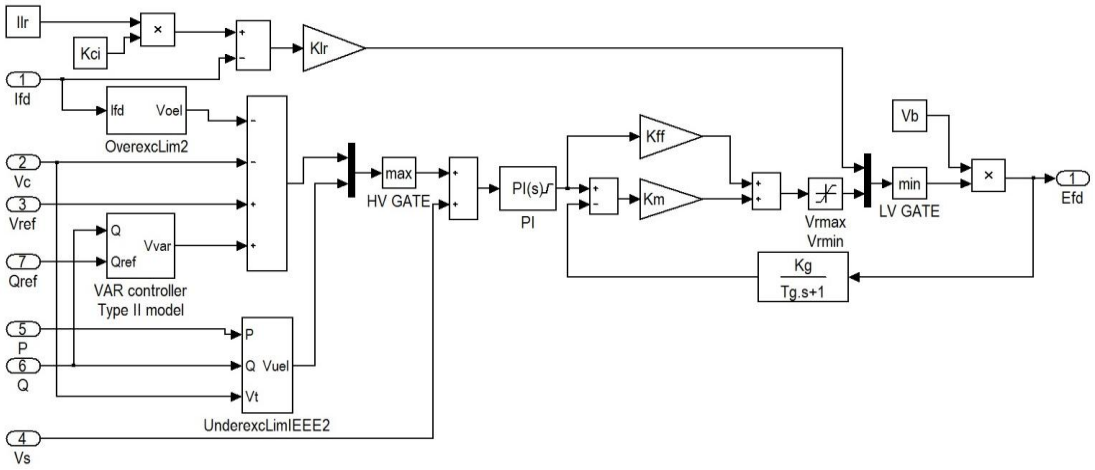

Figure 2. Model of the static excitation system.

According to the real HPP measurement practice [13], [20], a nonlinear relation between guide-vane position Y_v and active power P_e is modelled with a nonlinear function (15):

$$P_e = f(Y_v, dH) \tag{15}$$

Equ. (15) is the input to the transfer function of the water turbine (16):

$$\frac{P_m(s)}{P_e(s)} = \frac{1 + s \cdot A_{turb} \cdot T_{turb}}{1 + s \cdot B_{turb} \cdot T_{turb}} \tag{16}$$

while the output of the water turbine is mechanical power P_m, that presents the input to the synchronous generator.

In accordance with the IEC recommendations for the hydro turbines [13], parameter T_{turb} is the water inertia starting time, A_{turb}= -1 and B_{turb}= -0.5.

2.4 Block transformer

A three-phase 119/10.5 kV block transformer in the Yd11 winding connection with no core saturation is included in the model (Fig. 1). A function developed in Matlab *"TR_calc_param"* calculates resistances R_{1pu}, R_{2pu}, inductances L_{1pu}, L_{2pu} for both voltage windings, magnetization resistance R_{mpu} and magnetization inductance L_{mpu}. Besides the basic nominal transformer parameters (e.g. nominal power S_n, frequency f_n, …) obtained from the manufacturer [21], the calculated parameters present the input for the transformer block (SimPowerSystems library).

The resistances p.u. for the high-voltage and low-voltage windings are calculated with (17):

$$R_{1pu} = \frac{R_1}{Z_{b1}}, \quad R_{2pu} = \frac{R_2}{Z_{b2}} \tag{17}$$

where R_1, R_2, Z_{b1} and Z_{b2} are the phase resistances of the high-voltage winding, phase resistance of the low-voltage winding, base impedance of the high voltage-winding and base impedance of the low-voltage winding, respectively.

Assuming that reactances X_{1pu} and X_{2pu} of both windings are equal and that the transverse reactance in the short circuit has a very small value, the leakage inductance p.u. is:

$$L_{1pu} = X_{1pu} = \sqrt{Z_{kpu}^2 - (R_{1pu} + R_{2pu})^2} \tag{18}$$

It is equal for both windings $L_{1pu} = L_{2pu}$. Parameter Z_{kpu} denotes the short-circuit impedance in p.u.

Magnetization resistance R_{mpu} and inductance L_{mpu} are derived from an open-circuit test. The calculation of resistance R_{mpu} is expressed with (19) and (20):

$$R_{mpu} = \frac{R_{fe}}{Z_{b2}} \tag{19}$$

$$R_{fe} = \frac{U_{b2}^2}{\frac{P_0}{3}} \tag{20}$$

where R_{fe} presents the ohmic resistance of magnetization, U_{b2} denotes the phase voltage on the low-voltage side and P_0 is the power in the open-circuit state.

Magnetization inductance L_{mpu} is expressed as (21):

$$L_{mpu} = \frac{X_\mu}{Z_{b2}} = \frac{\frac{U_{b2}}{I_\mu}}{Z_{b2}} \tag{21}$$

where X_μ is the reactance of magnetization and I_μ denotes the inductive part of the magnetization current, calculated as follows:

$$I_\mu = \sqrt{I_{0f}^2 - I_{fe}^2} \tag{22}$$

with the common current in open-circuit I_{0f} and resistive part of current I_{fe} at magnetization.

2.5 110 kV electrical network

The three-phase 110 kV transmission line sections with lumped parameters in the vicinity of the Mavčiče HPP are included in the dynamic model. Assuming that the three phases are balanced, R, L and C, the line parameters are applied as the positive and zero sequence parameters, taking into account the inductive and capacitive couplings between the phases and the ground [22].

Table 1 presents the parameters of the 110 kV transmission line sections with length *l*, voltage sources with three-phase short circuit power S_{ks} and the RLC loads included in the electrical network. Besides the Mavčiče HPP, four important connections to the switchgears are analysed in the model: the *KL* (Kleče), *ME* (Medvode), *LAB* (Labore) and *OKR* (Okroglo) switchgears.

Table 1: Parameters of the 110 kV electrical network [24] included in the model

Functional part	S_{ks} **[MVA]**	***l*** **(km)**	P_i **[MW]**	Q_i **[MVAr]**
3f U_s KL-ME	456	/	-9.3	-2.7
3f PI line KL-ME	/	8.310	/	/
3f U_s ME	29.5	/	9.05	2.02
3f RLC load ME	/	/	13.55	1.61
3f PI line ME-MA	/	12.66	/	/
HPP MA gen. 1	/	/	3	2
HPP MA gen. 2	69.5	/	7	4.28
3f PI line MA-LAB	/	9.411	/	/
3f U_s LAB-MA	655	/	0	0
3f RLC load LAB	/	/	22.18	3.34
3f PI line LAB-OKR	/	5.780	/	/
3f U_s OKR-LAB	222	/	26.16	-1.36

The voltage sources and RLC loads are set to the initial values of P_i and Q_i, identical to the observed measurements taken on the 21st January 2015. The

results are recalculated with a load-flow tool in the SimPowerSystems (Newton-Raphson iterative method [23]) and show appropriate matching with the real measurements.

3 SIMULATION RESULTS AND VALIDATION OF THE MODEL

The proposed HPP dynamic model is implemented with the real-system initial values of the Mavčiče HPP generator 1 with subsystems. The generator RMS (L_1, L_2 and L_3) currents are set to: I_{gm}= 0.143 p.u., line RMS voltage U_{gm}= 1.009 p.u., active power P_{gm}= 0.12 p.u. and reactive power Q_m = 0.08 p.u.

In the excitation system, the initial field voltage is set to U_{fm}= 1.117 p.u., the voltage reference V_{ref}= 1.0105 p.u. and the reactive-power reference Q_{ref}= 0.08 p.u.

The active-power reference of the turbine controller presented in Equ. (13) is set to P_{ref}= 0.12 p.u. (the same as the feedback of generator active power P_{gm}), while the rotation-speed reference is w_{ref}= 1 p.u. (the generator is synchronized to the electrical network). The guide-vane opening of the water turbine is Y_v= 0.277 p.u., wheras the runner opening is positioned at Y_g=0 p.u., with the reference to the ratio $\frac{Y_g}{Y_V}$ and head *dH* from Equ. (14).

The model simulation presents a stepwise increase and decrease in the generator active power (Fig. 3) at a constant reactive power and frequency in a 1000 s time frame (observed from 30 to 1030 s).

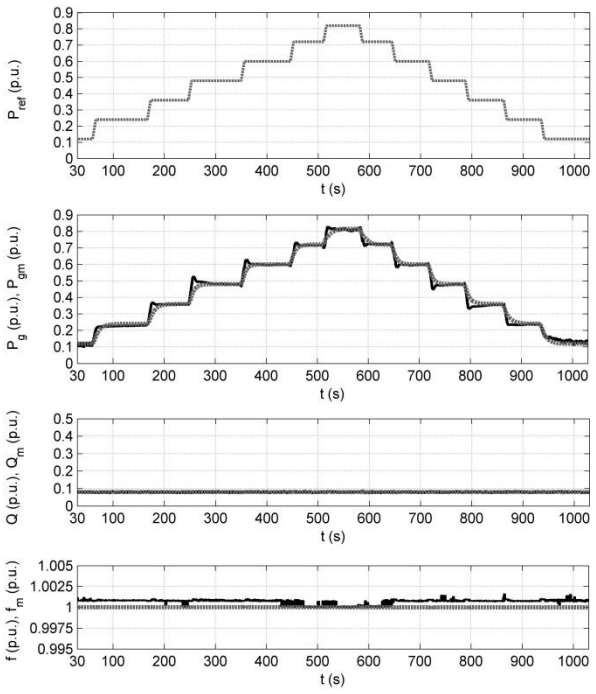

Figure 3. Reference of active power P_{ref} (measured and simulated), measured generator active power P_g, reactive power Q and frequency f depicted with a solid line, while the results of model P_{gm}, Q_m and f_m are presented with a dashed line.

The same reference of the active power is gradually changed on the SCADA touch screen of HPP and in simulation for a 0.12 step p.u. depicted in Fig. 3 (top graph). Active power of the generator model P_{gm} (dashed line) and measured generator active power P_g (solid line) follow the referential signal to minimize the error from Equ. (13) presented in Fig. 3 (second graph). The reference for the reactive power Q_{ref}= 0.08 p.u. is kept constant during the simulation, and consequently modelled reactive power Q_m (Fig. 3, third graph, dashed line) and measured reactive power Q (solid line) remain at 0.08 p.u. Modelled frequency of the generator f_m, presented in Fig. 3 (bottom graph) with a dashed line as well as measured frequency f depicted with a solid line remain constant due to the stiffness of the 110 kV network.

Fig. 4 shows matching of the results of modelled generator current I_{gm}, line voltage U_{gm} and 110 kV transformer phase voltage U_{mL1} with the real system measurements I_g, U_g and U_{L1}. The dynamic response of the generator active power P_{gm} (Fig. 3) is proportional to generator current I_{gm} (Fig. 4, top graph). Simulated line voltage of the generator U_{gm} (Fig. 4, second graph) remains constant due to unchanged generator reactive power Q_m. Simulated L1 phase voltage U_{mL1} on the primary side of the 119/10.5 kV transformer is shown on the bottom graph of Fig. 4.

The model of excitation field current I_{fm} and voltage U_{fm} is shown in Fig. 5. Direct current I_{fm} that magnetizes the rotor of the generator (Fig. 5, top graph) is controlled with direct voltage U_{fm} (Fig. 5, bottom graph) via a static thyristor excitation system. Compared to the real excitation system (U_f and I_f, solid line), 0.04 p.u. lower field voltage U_{fm} (Fig. 5, second graph, dashed line) is obtained at highest active power P_g= 0.82 p.u. (at time t= 560 s).

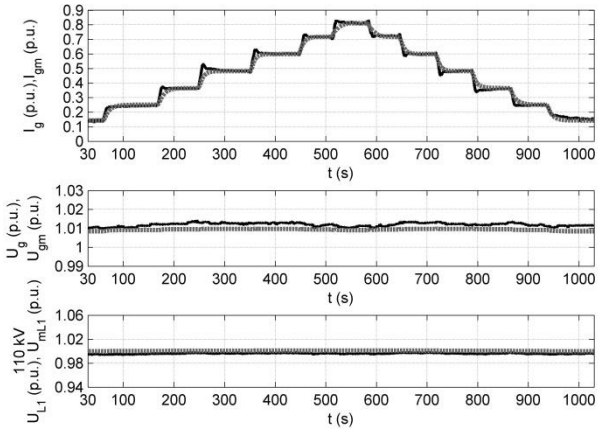

Figure 4. Comparison between measured generator L1 RMS current I_g, line (L1-L2) RMS voltage U_g (solid lines) and the output of the generator model with I_{gm} and U_{gm} (dashed lines). The 110 kV L1 RMS voltages of the transformer U_{L1}

(measurement – solid line) and simulated U_{mL1} (dashed line) are depicted in the bottom graph.

The response of the controlled water-turbine model is presented in Fig. 6 (dashed line) with guide-vane Y_{vm} and runner Y_{gm} opening. The measurements of both openings (Y_v and Y_g) are presented with a solid line. The displacement of the guide-vane opening Y_{vm} (Fig. 6, top graph) that participates in synchronization, emergency shut-down functions and load rejection are faster than the runner change at opening. According to the increase in the Y_{vm} up to 0.45 p.u., active power P_{gm} increases, whereas the runner (Fig. 6, second graph) stays in a closed position. At higher referential active power P_{ref} (Fig. 3, top graph, from 0.48 p.u. up to 0.82 p.u.), runner opening Y_{gm} increases to provide more water through the turbine at consequently higher active power P_{gm}. In the simulation, real net head H_m (Fig. 6, bottom graph) is included to achieve the real cirumstances.

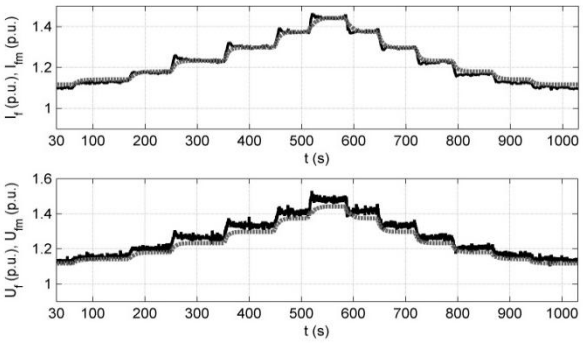

Figure 5. Comparison between measured excitation current I_f and voltage U_f (solid line) and model of the excitation system with I_{fm} and U_{fm} (dashed line).

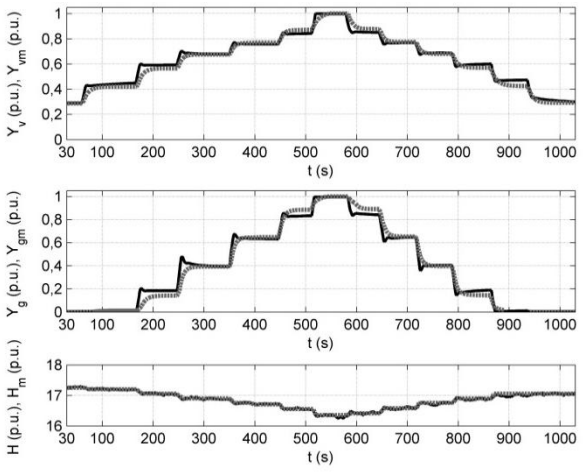

Figure 6. Measurement of Kaplan turbine guide vane Y_v and runner opening Y_g (solid line) and model responses Y_v and Y_g (dashed line) at the same water conditions (equal heads H=H_m).

During the increase in generator active power P_m, net head H_m (Fig. 6, bottom graph) is decreased (from 17.25 m to 16.25 m) due to the lowered lake water level and increased HPP tail water.

4 IMPACT OF THE HPP OPERATION ON THE 110 KV ELECTRICAL NETWORK

Referring to the proposed model of the 110 kV electrical network from Sec. 2.5 and initial state parameters (Table 1), the impact of the changed active power on the 110 kV network and frequency deviation in the range ±0.025 p.u. with the same initial condition is presented in Fig. 7.

In the first case (at a constant frequency), the response of simulated active power P_m (grey dashed line) compared to measurements P (black solid line) is depicted in Fig. 7 on graphs (c), (d), and (e) for the Kleče-Medvode, Labore-Mavčiče and Okroglo-Labore 110 kV transmission lines, respectively. At the beginning of the simulation, the direction of power flow was from the Okroglo to the Kleče switchgear (positive P_m at Okroglo-Labore and negative P_m at Kleče-Medvode). The sink of the modelled active power on the Kleče-Medvode transmission line increases from P_m= -9.3 MW to -14.5 MW, while active power P_m at Labore-Mavčiče changes its direction (from source P_m= 3.95 MW to sink P_m= -6.55 MW).

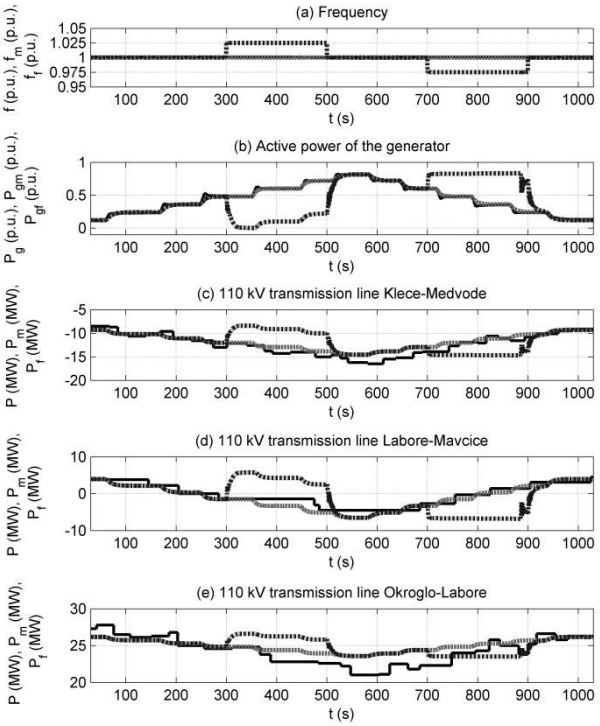

Figure 7. Impact of the HPP Mavčiče operation on the Kleče-Medvode, Labore-Mavčiče and Okroglo-Labore 110 kV transmission lines at constant frequency f_m (grey dashed line) and changed frequency f_f (black dashed line). The measurements of frequency f (graph (a)), generator power P_g (graph (b)) and active power P on the transmission lines (graphs (c), (d) and (e)) are depicted with a solid black line.

On the Okroglo-Labore transmission line, the source of active power P_m decreases (from P_m= 26.2 MW to 23.6 MW). The comparison presented in Fig. 7 shows a correct matching between the simulated and actual mesurements. The largest difference between the model and measurement results ΔP= -3.6 MW is noticed on the Labore-Mavčiče transmission line at time t= 470 s).

In the second case, the increase in frequency f_f (Fig. 7, graph (a), black dashed line) for +0.025 p.u in the time range from 300 s to 500 s and decrease of -0.025 p.u. from 700 to 900 s is simulated. At the increase in frequency f_f, simulated active power of generator P_{gf} decreases from 0.48 p.u. to -0.02 p.u. (Fig. 7, graph (b), black dashed line) due to the steady-state droop R= 0.05 p.u. from Equ. (13). Consequently, the sink of the active power on the Kleče-Medvode transmission line (Fig. 7, graph (c), black dashed line) decreases for 3.6 MW, whereas the source of the active power on the Labore-Mavčiče transmission lines (Fig. 7, graph (d), black dashed line) and Okroglo-Labore (Fig. 7, graph (e), black dashed line), increases for 7.1 MW and 1.8 MW, respectively.

At the time of 700 s, simulated frequency f_f decreases for -0.025 p.u. (Fig. 7, graph (a)) and active power P_{gf} (Fig. 7, graph (b)) increases to 0.98 p.u., however it is limited to 0.82 p.u. due to the turbine power range. The transmission line active power (Fig. 7, graphs (c), (d) and (e)) changes oppositely to the results obtained at the frequency increase.

The total change in the transmission-line active power (12.5 MW) is equal to the change in the generator active power (0.5 p.u.) due to the frequency deviation.

5 CONCLUSIONS

A complex dynamic model of a HPP integrated in a 110 kV electrical network is proposed. The basic properties of the synchronous generator, static excitation system, water turbine, turbine controller, power transformer and simplified 110 kV network are realized in Matlab/Simulink with the SimPowerSystems library based on real-system parameters and IEEE recommended practice.

The results of using the developed dynamic model and its subsystems are validated with measurements taken at the Mavčiče HPP and show appropriate matching of the responses. The observed changes in the active power from P_m= 0.12 p.u. to 0.82 p.u. strongly affect the power flow on the 110 kV transmission lines. The results obtained for the Labore-Mavčiče transmission line reveal a change in the active-power flow direction from P_m= 3.95 MW to P_m= -6.55 MW.

When simulating the frequency deviation, the turbine controller with a steady-state droop parameter appropriately changes the generator active power without menacing the network stability.

The presented dynamic model uses a useful software equipment for further development of the HPP control systems, study of the impact on electrical network and allows to simulate the tests which are difficult to evaluate on a real power system.

REFERENCES

[1] The Institute of Electrical and Electronics Engineers (IEEE), "IEEE Std 421.5-2005 – IEEE Recommended Practice for Excitation System Models for Power System Stability Studies", New York, USA, 2006.

[2] Shayeghi H., Shayanfar H. A., Jalili A. "Load frequency control strategies: A state-of-the-art survey for the researcher", *Energy Conversion and Management*, 50(2009), pp. 344-353, 2009.

[3] Kishor Nandar, Saini R.P., Singh S.P., "A review on hydropower plant models and control", *Renewable & Sustainable Energy Reviews*, 11(2007), pp. 776-796, 2007.

[4] Naghizadeh R.A., Jazebi S., Vahidi B., "Modelling hydro power plants and tuning hydro governors as an educational guideline", *International review on Modelling and Simulation*, 5(4), pp. 1780-1790, 2012.

[5] Singh Parmar K.P., Majhi S., Kothari D.P., "Load frequency control of a realistic power system with multi-source power generation", *Electrical Power and Energy Systems*, 42(2012), pp. 426-433, 2012.

[6] Prakash Surya, Sinha S.K., "Simulation based neuro-fuzzy hybrid intelligent PI control approach in four-area load frequency control of interconnected power system", *Applied Soft Computing*, 23(2014), pp.152-164,2014.

[7] Pan Indranil, Das Saptarshi, "Frequency domain design of fractional order PID controller for AVR system using chaotic multi-objective optimization", *Electrical Power and Energy Systems*, 51(2013), pp.106-118, 2013.

[8] Prillwitz Fred, Al-Ali Salah Eddin, Haase Torsten, Weber Harald, Saqe Lutfi, "Simulation model of the hydro power plant Shkopeti", *6th EUROSIM Congress on Modelling and Simulation*, 9.-13. September, 2007, Ljubljana, Slovenia.

[9] International Electrotechnical Commission (IEC), "IEC 60308:2005 Hydraulic Turbines—Testing of Control Systems", 2nd ed., Geneva, Switzerland, 2005.

[10] International Electrotechnical Commission (IEC), "IEC 61362: 2012 Guide to Specification of Hydraulic Turbine Control Systems", 2nd ed.; Brussels, Belgium, 2012.

[11] International Electrotechnical Commission (IEC), "CLC/TR 60034-16-2:2004: Rotating electrical machines-Part 16-2: Excitation systems for synchronous machines – Models for power system studies", Brussels, Belgium, 2004.

[12] International Electrotechnical Commission (IEC), "CLC/TR 60034-16-3:2004: Rotating electrical machines – Part 16-3: Excitation systems for synchronous machines – Dynamic performance ", Brussels, Belgium, 2004.

[13] International Electrotechnical Commission (IEC), "Draft IEC 61970: Energy Management System Application Program Interface (EMS-API) – Part 457: Common Information Model for Dynamics Profile", 1st ed., Brussels, Belgium, 2013.

[14] Avdakovic Samir, Bosovic Adnan, "Impact of charging a large number of electric vehicles on the power system voltage stability", *Elektrotehniški vestnik*, 81(3), pp. 137-142, 2014.

[15] Volkanovski Andrija, Čepin Marko, Mavko Borut, "Optimization of reactive power compenzation in distribution networks", *Elektrotehniški vestnik,* 76(1-2), pp. 57-62, 2009.

[16] Gjorgiev Blaže, Čepin Marko, Volkanovski Andrija, Kančev Duško, "Multi-objective power-generation scheduling: Slovenian power system case study", *Elektrotehniški vestnik*, 80(5), pp. 222-228, 2013.

[17] Krause Paul C., *Analysis of Electric Machinery,* McGraw-Hill Book Company, New York, 1986.

[18] Rade Končar, *Ispitivanje sinhronog generatora HE "Mavčiče"*, Zagreb, 1988.

[19] Grigsby Leonard L., *Power system stability and control*, CRC Press Taylor & Francis Group, 2nd ed., Boca Raton, 2007.

[20] Andino Hydropower Engineering d.o.o., *HE Mavčiče, 2 Kaplan agregata – Turbinski regulator in ostala oprema 1.01.1134*, Ljubljana, 2011.

[21] Kolektor ETRA d.o.o., *Tehnična dokumentacija za transformator tip BT 25000-119/10,5 YNd5*, Ljubljana, 2013.

[22] Hydro-Québec, TransÉnergie Technologies, *SimPowerSystems for use with Simulink*, The MathWorks, Version 3, Natick, 2003.

[23] Glover J. Duncan, Sarma Mulukutla S., Overbye Thomas J., *Power system analysis and design*, Cengage Learning, 4th ed., Stamford, 2010.

[24] Elektroinštitut Milan Vidmar, *Raziskave kratkostičnih razmer v slovenskem EES do leta 2004*, Ljubljana, 1999.

Klemen Nagode received his Diploma Engineer degree in Electrical Engineering from University of Ljubljana, Slovenia in 2007. He is currently a postgraduate student at the Faculty of Electrical Engineering and works in the Department of Electrical Engineering of Savske elektrarne Ljubljana d.o.o. His research interests include automation, measurements, control systems, modelling and simulation of power systems.

Boštjan Murovec is an associate professor at the Faculty of Electrical Engineering of University of Ljubljana, Slovenia. He gained his B.Sc, M.Sc and D.Sc. degrees in electrical engineering in years 1996, 1999 and 2002, respectively. His research interests include machine vision, bioinformatics, combinatorial optimization and embedded systems.